Osteoconductive Property of a Mechanical Mixture of Octacalcium Phosphate and Amorphous Calcium Phosphate

Kazuhito Kobayashi,[†,‡] Takahisa Anada,[‡] Takuto Handa,[†,‡] Naofumi Kanda,[†,‡] Mariko Yoshinari,[‡] Tetsu Takahashi,[†] and Osamu Suzuki*[,‡]

[†]Division of Oral and Maxillofacial Surgery and [‡]Division of Craniofacial Function Engineering, Tohoku University Graduate School of Dentistry, Sendai, Miyagi 980-8575, Japan

ABSTRACT: The present study was designed to investigate the extent of osteoconductive property of a mechanical mixture of octacalcium phosphate (OCP) and amorphous calcium phosphate (ACP). OCP was mixed with ACP in granules that had a diameter of 300 and 500 μm, respectively, and at 25, 50, or 75 wt %. The physicochemical characteristics and the osteoconductive properties of the mixtures were compared with OCP alone or ACP alone through implantation into rat critical-sized calvaria

defects for up to 12 weeks and simulated body fluid (SBF) immersion for 2 weeks. The mixtures of OCP and ACP, in particular the OCP 25 wt % and ACP 75 wt % (O25A75), had higher radiopacity compared to ACP and OCP alone. O25A75 induced greater enhancement of bone regeneration than ACP alone at 8 weeks and that than OCP alone at 12 weeks. X-ray diffraction and Fourier transform infrared (FTIR) analyses of the retrieved mixtures showed that ACP, OCP, and O25A75 tended to convert to hydroxyapatite (HA) after the implantation, while the structure of OCP remains without complete conversion after SBF immersion. Analyses by FTIR curve fitting of the solids and the degree of supersaturation of the SBF supported the observation that the existence of ACP enhances the kinetics of the conversion. Scanning electron microscopy found that the surface of O25A75 had distinct characteristics with OCP and ACP after SBF immersion. The results suggest that the extent of the osteoconduction of OCP could be controlled by the copresence of ACP most probably through the prevailing dissolution−precipitation of the surface of ACP crystals to form HA.

KEYWORDS: octacalcium phosphate (OCP), amorphous calcium phosphate (ACP), hydoroxyapatite (HA), conversion, bone regeneration
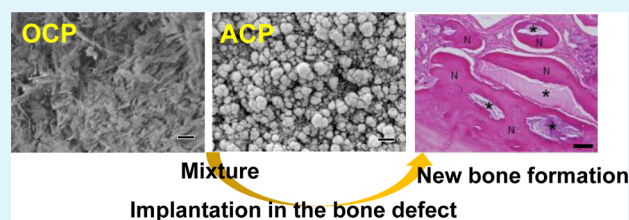
■ INTRODUCTION

Previous studies have shown that synthetic octacalcium phosphate (OCP; $Ca_8H_2(PO_4)_6 \cdot 5H_2O$) enhances bone regeneration to a greater extent than calcium-deficient hydroxyapatite (Ca-deficient HA) if implanted in a critical-sized rat calvaria defect model.[1] The Ca-deficient HA, which is a non-stoichiometric form of HA ($Ca_{10}(PO_4)_6(OH)_2$), was obtained through a hydrolysis reaction from the original OCP and therefore considered a suitable control material to OCP.[1] X-ray diffraction analysis of the retrieved materials from the implanted site confirmed that the crystal phase of OCP is progressively hydrolyzed (converted) to that of low crystalline HA in situ over time.[1] We previously proposed that the higher osteoconductive properties of OCP could be acquired as a result of physicochemical conversion into HA.[1] This hypothesis was further supported by the in vitro observation that osteoblastic differentiation of mouse bone marrow stromal cells seeded directly on OCP crystals is enhanced in a dose-dependent manner with a concomitant increase in the mRNA levels of osteoblast differentiation marker genes.[2] Moreover, a similar conversion of OCP into HA occurs during the incubation in the medium.[1] However, the mechanism by which the conversion of OCP itself affects the extent of the osteoconductivity of this material remains unknown.

OCP has been advocated as a precursor to bone apatite crystals.[3] The structure of OCP consists of apatite layers stacked with hydrated layers in an alternating fashion.[4] In addition, the phase of OCP was shown to be a precursor to HA based on experimentally prepared calcium and phosphate solutions at physiological conditions.[5] OCP is considered to be a direct precursor to HA because the process of HA formation from OCP only consists of the OCP and HA phases.[6,7] Once initiated, the conversion advances spontaneously, irreversibly, and topotaxially without changing its original crystal morphology.[4,6,7] When OCP is converted to HA, the OCP crystals absorb calcium ions and release phosphate ions into the surrounding solution, which corresponds to the progressive increase of the solid molar ratio in calcium and phosphorus.[6,8] This conversion induces progressive changes in adsorption affinity of the crystals for serum proteins.[7,9] OCP has a surface pool of labile HPO_4 that exists as reversibly exchangeable acidic ions on and in the crystal lattice, which progressively decreases during the conversion to HA.[10] The conversion rate of OCP to HA is predominantly controlled by the degree of super-

saturation with respect to HA and OCP, which is given a numerical value based on the concentrations of calcium and phosphate ions as well as the ion pairs that form with physiologically ubiquitous inorganic ions, such as Mg ions under neutral pH.[8,11] The presence of fluoride ions affects the conversion of OCP because fluoride promotes the formation of fluoridated HA, which has lower solubility than HA.[12] If the conversion of implanted OCP can be artificially regulated by such environmental factors in vivo, then it is of interest to learn whether the osteoconductivity of OCP could be strengthened or weakened.

Amorphous calcium phosphate (ACP; $Ca_3(PO_4)_2 \cdot nH_2O$), which was recently recognized to be amorphous tricalcium phosphate (ATCP), is considered to be another precursor to HA formation in bone mineralization.[13-15] It is known that ACP has greater solubility than OCP under physiological conditions.[5,16] ACP is formed as the first mineral solid phase from supersaturated calcium and phosphate solutions[14] and then crystallizes to an OCP-like phase that subsequently transforms to HA.[5] The latter phase is the most thermodynamically stable phase in calcium phosphate compounds at physiological pH.[6] Calcium phosphate cluster theories have been proposed to explain the structural and chemical relationships between these precursor phases and HA, in which HA formation occurs through the nucleation of calcium phosphate clusters with subsequent transformation into HA through aggregation of the clusters.[17-19] The structural unit of the cluster, which preserves ACP and OCP, is present in the structural domains of the HA that forms.[19]

It has been shown that synthetic ACP shows a bioactive property if used as a scaffold material in hard tissue formation.[20-24] Our previous study indicated that ACP (ATCP, Ca/P molar ratio 1.5) as well as OCP enhances bone formation more than nonsintered and nonstoichiometric HA (Ca/P molar ratio 1.5) and stoichiometric HA (Ca/P molar ratio 1.67) when compared to a subperiosteal onlay implantation onto murine calvaria.[22] In the present study, we hypothesized that if ACP is present together with OCP, then the conversion and the osteoconductivity of OCP are controlled possibly due to the delivery of calcium and phosphate ions from ACP under physiological pH.[5,16] The present study was therefore designed to investigate whether the conversion of OCP is controlled in the copresence of ACP and whether the osteoconductivity of OCP is strengthened in vivo.

■ EXPERIMENTAL SECTION

Synthesis and Preparation of OCP, ACP, and Ca-Deficient HA. OCP was synthesized by mixing calcium and phosphate solutions under constant pH 5−6 and temperature at 70 °C according to a well-established wet synthesis method previously reported.[22] The precipitate was recovered from the reacting solution and was then washed by water several times and dried at 105 °C for subsequent use. ACP was synthesized by a method by Eanes et al.[14] with modification as reported previously.[22] Briefly, calcium solution (nitric salt solution) was rapidly mixed with phosphate solution (ammonium salt solution) at room temperature.[22] The precipitate was immediately recovered from the reacting solution and was then washed by dilute ammonium water several times and lyophilized for subsequent use. Ca-deficient HA, as a control for the analysis of materials, was obtained by the hydrolysis of the original OCP precipitate, just after the synthesis of OCP, for 48 h at 65 °C in hot water.[1] The method to obtain Ca-deficient HA and the characteristics of this material have been well documented previously.[1] The granules were prepared by lightly grinding the dried OCP or ACP cake using a mortar and pestle, and then they were passed through a standard testing sieve. The granules

with diameters ranging from 300 to 500 μm were prepared. Both the granules were mixed at different ratios of OCP:ACP as follows: 100:0, 75:25, 50:50, 25:75, and 0:100 (Table 1). The mixtures were agitated by a rotary shaker for 1 h for dispersing them from each other.

Table 1. Mixing Ratios between OCP and ACP

OCP wt %	ACP wt %	designation
100	0	OCP
75	25	O75A25
50	50	O50A50
25	75	O25A75
0	100	ACP

Characterization of OCP and ACP. OCP and ACP were characterized by powder X-ray diffraction (XRD) and Fourier transform infrared spectroscopy (FTIR). XRD patterns were recorded using a step scanning at 0.05 degree intervals from 3.0 degrees to 60.0 degrees, with Cu Kα X-rays on a diffractometer (Mini Flex; Rigaku Electrical Co., Ltd., Tokyo, Japan) at 30 kV and 15 mA. The 2θ range measurement included the main reflection (100) of OCP at 4.7° 2θ. Joint Committee for Powder Diffraction Standard (JCPDS) numbers 26-1056A9 for OCP and 9-432 for HA were utilized to identify their crystalline phases. The FTIR spectrum of OCP was obtained by FTIR spectroscopy (FT/IR-6300; JASCO Corporation, Tokyo, Japan) with the sample diluted in KBr over a range of 4,000−400 cm^{-1} with 4 cm^{-1} resolution. The morphology of crystals and granules was examined using a JEOL analytical scanning electron microscope (SEM) JSM-6390LA (Tokyo, Japan) operating at an accelerating voltage of 10 kV. Au−Pd sputtering was performed using the powder samples before the observation.

Implantation of OCP and ACP Granules and the Mixed Granules. Twelve-week-old male Wistar rats (SLC, Hamamatsu, Shizuoka, Japan) were used. The principles of laboratory animal care were followed as well as the national laws. All procedures were approved by the Animal Research Committee of Tohoku University. The experimental rats were anesthetized with intraperitoneal sodium pentobarbital (50 mg/kg) supplemented by ether inhalation. A skin incision was made aseptically along the bilateral temporal line and the middle of the forehead, and the dissection was continued to the calvarium. The periosteum of the calvarium was ablated, and a full-thickness standardized trephine defect (9 mm in diameter) was made in the calvarium under continuous saline buffer irrigation. Extreme care was exercised to avoid injury to the midsagittal blood sinus and dura mater. The OCP or ACP or the mixed granules were implanted into the trephine defect. As a negative control, untreated animals were processed in the same way except that no implantation was made after the defects were created. After the defects were treated, the ablated periosteum and skin were repositioned and sutured, respectively.

Radiographic Analysis. Rats were anesthetized with an intra-peritoneal injection of sodium pentobarbital (50 mg/kg) supplemented with ether inhalation. The rats were then sacrificed, and the implants were resected with the surrounding calvaria bones. The tissues were immersed in 4% paraformaldehyde in 0.1 M PBS (pH 7.4) for tissue fixation and incubated overnight at 4 °C. The specimens were radiographed using a micrography unit (Softex CMBW-2, Softex, Tokyo, Japan) with X-ray film (FR; Fuji photo film, Tokyo, Japan) under standardized conditions (20 kV, 5 mA, 20 s), in which OCP and ACP showed no radiopacity. The percentage of X-ray opacity in the defect (Radiopacity%) was calculated as the area of radiopacity per area of the defect originally created by trephination ×100. The radiopacity% was quantified on a computer using Scion Image public domain software (Scion Corporation, Frederick, MD).

Tissue Preparation. After the radiographs were taken, the samples were decalcified in 10% ethylenediaminetetraacetic acid in 0.01 M phosphate buffer, pH 7.4, for 2−4 weeks. The samples were dehydrated in a graded series of ethanol and embedded in paraffin. The center of the defect in calvaria was extracted and sectioned coronally with a thickness of 5 μm. The sections were stained with

22603

dx.doi.org/10.1021/am5067139 | ACS Appl. Mater. Interfaces 2014, 6, 22602−22611

hematoxylin and eosin (H&E) by a standard method, and photographs were taken with a photomicroscope (Leica DFC300 FX, Leica Microsystems Japan, Tokyo, Japan). Light micrographs of the sections stained with H&E were used for histomorphometric measurements. Photographs projecting the overall defect were taken for each specimen. The percentage of newly formed bone in the defect (n-Bone%) was calculated as the area of newly formed bone per area of the defect originally created by trephination ×100. The n-Bone% was quantified on a computer using Scion Image public domain software (Scion Corporation, Frederick, MD).

Evaluation of Change in the Crystal Phase in Vivo. The implanted granules in the rat calvaria were examined for XRD. The granules were retrieved from rat calvaria bone defects of two to four rats at 2 weeks postimplantation using tweezers so as to exclude as much of the soft tissue around the implanted granules as possible. The granules were ground using a mortar and pestle after lyophilization. The XRD analysis was performed under the same conditions used for the characterization of the crystals as described above.

Structural Changes of Crystals in SBF. SBF solution was prepared according to a method previously described[25] by dissolving a reagent grade of sodium chloride, sodium hydrogen carbonate, potassium chloride, dipotassium hydrogen phosphate trihydrate, magnesium chloride hexahydrate, and calcium chloride dihydrate in purified water. The solution was then buffered with trihydroxymethyl aminomethane and hydrochloric acid to attain pH 7.4 at 37.0 °C. The OCP, ACP, and their mixtures (50 mg) were immersed in 50 mL of the fresh SBF (solid/solution ratio 1 mg/1 mL) in separate plastic tubes placed in a 37.0 °C water bath. The experiment was performed with constant stirring to avoid possible pH change in particular the pH increase by the effect of ACP dissolution. The immersed granules were collected after 1 and 2 weeks, washed with water, and then lyophilized for XRD observation. The concentration of calcium and inorganic phosphate ions in the supernatants after the immersion in the SBF solution was determined quantitatively using Calcium E and Phosphor C tests (Wako Pure Chemical Industries, Osaka, Japan), respectively.

FTIR Spectroscopy and Curve Fitting Analysis. The FTIR spectrum of the composites was obtained by FTIR spectroscopy (FT/IR-6300; JASCO Corporation, Tokyo, Japan) with the dilution in potassium bromide over a range of $4000-400$ cm^{-1} with 4 cm^{-1} resolution. The intensities of apatitic OH and HPO$_4$ or nonapatitic HPO$_4$ in FTIR spectra were estimated by employing curve-fitting with Spectra Manager Version 2.10 (Curve fitting Version 2.05). An IR band ratio between 450 and 700 cm^{-1} was used according to a method reported by Rey et al.[21,26]

Estimation of the Degree of Supersaturation. Degree of supersaturation (DS) of SBF and those after immersing OCP, O25A75, and ACP were calculated to estimate the dissolution of granules with respect to OCP, HA, and dicalcium phosphate dihydrate (DCPD) in the solution. The DS value is the numerical value obtained by dividing the ionic product with the solubility product for objective calcium phosphates. The DS corresponds to the point at which the solution is saturated for a specific calcium phosphate salt. The DS calculations were made for 37 °C using a modification of ion speciation software previously developed.[27,28] The DS value is in general calculated by the analytical concentration of Ca, Mg, Na, K, P, Cl, and F as well as the pH value combined with the three mass balance equations for [Ca], [P], and [Mg], according to previous reports.[11,28,29] The calculation also assumes the presence of HCO$_3^-$ in the fluid. The ion pairs included in the calculation were CaH$_2$PO$_4^+$, CaHPO$_4^0$, MgHPO$_4^0$, CaHCO$_3^+$, and MgHCO$_3^+$. The DS was defined in terms of the mean ionic activity product with respect to HA, OCP, and DCPD. In the present study, the concentration of Ca^{2+} and inorganic phosphate (Pi) obtained by chemical analyses was used for the SBF. Ion concentrations of 142 mM Na, 5 mM K, and 1.5 mM Mg of the SBF composition[25] were used. The pH value 7.4 and the physiologic partial pressure 1.86% in carbonate were used for the calculation. The solubility product constants used were 7.36×10^{-60} for HA[12] and 2.51×10^{-49} for OCP.[30]

Statistical Analysis. All values were reported as the means ± standard deviations. All experiments were performed at least three

times and showed reliable reproducibility. Statistical differences among specimens were evaluated by the Tukey-Kramer multiple comparison analysis. A value of $p < 0.05$ was regarded as statistically significant.

■ RESULTS

Characteristics of OCP and ACP. Figure 1 shows SEM photographs of OCP and ACP granules. OCP exhibited a platy
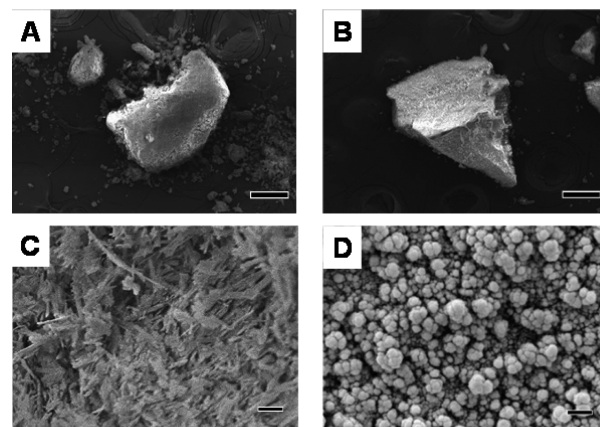

Figure 1. Scanning electron micrographs of OCP (A, C) and ACP (B, D). Bars = 100 μm (A, B) and 1 μm (C, D).

morphology of several micrometers in length and had the same characteristics as previously reported (Figure 1A and C).[7] ACP granules consisted of densely packed spherelike nanocrystals (Figure 1B and 1D).

Figure 2a shows the XRD pattern of OCP. All reflections of XRD observed for OCP, including the characteristic (1 0 0)
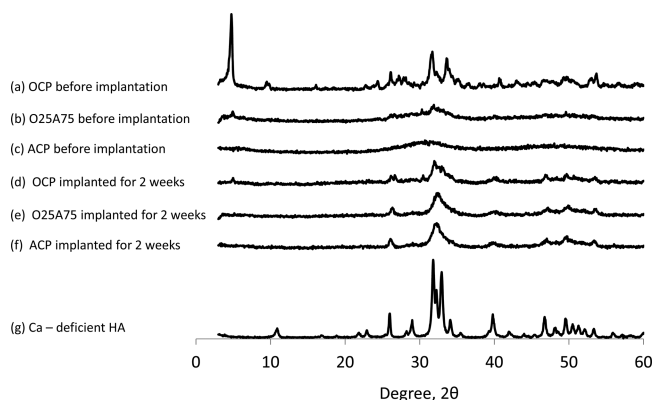

Figure 2. X-ray diffraction patterns of OCP before implantation (a), O25A75 before implantation (b), ACP before implantation (c), OCP implanted for 2 weeks (d), O25A75 implanted for 2 weeks (e), ACP implanted for 2 weeks (f), and Ca-deficient HA (Ca/P molar ratio: 1.56) (g).

reflection at $2\theta = 4.9°$ and (7 0 0) reflection at $2\theta = 33.6°$, corresponded well to those expected from an OCP structure.[1,31] Figure 2c shows the XRD pattern of ACP. The ACP powder showed a broadened peak around 30°, which was characteristic of an amorphous state.[22]

Structural Changes of OCP, ACP, and Their Mixture in Vivo. Figure 2 also shows the XRD patterns of the OCP, ACP, and their mixture before (Figure 2b) and 2 weeks after implantation (Figures 2d−2f) in rat calvarial defects and also Ca-deficient HA as a control material (Figure 2g). The

structure of all samples tended to convert to that of HA. The conversion of implanted ACP and the mixture seemed to advance faster than the implanted OCP.

Radiographic Examination 8 Weeks Postimplantation. In the untreated defects, radiopacity was observed along the defect margins at week 8 (Figure 3a). In the implanted

(a) Untreated   (b) ACP   (c) O25A75

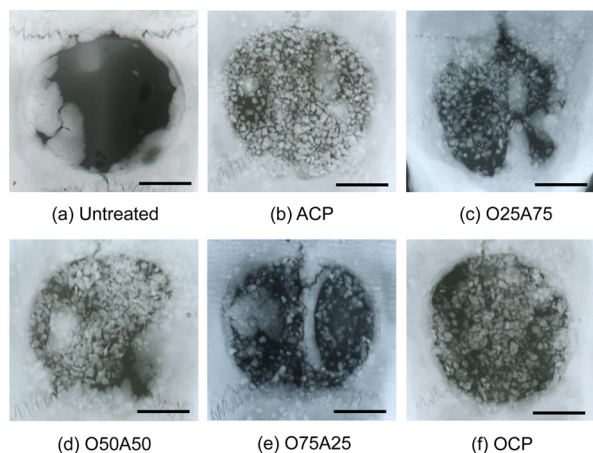(d) O50A50   (e) O75A25   (f) OCP

Figure 3. Radiographs of rat calvarial defects of untreated control (a) or with implantation of ACP (b), O25A75 (c), O50A50 (d), O75A25 (e), or OCP (f) for 8 weeks. Bars = 3 mm.

groups, isolated granulose radiopacity was scattered throughout the defect, showing a distinct degree in the radiopacity (Figure 3b–Figure 3f). Figure 4 shows the analytical results of
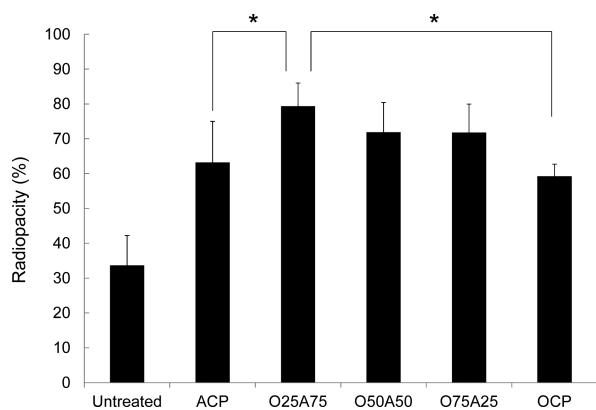

Figure 4. Quantitative analysis of the percentage of radiopacity in the defect at 8 weeks postimplantation of ACP, OCP/ACP mixtures, or ACP. Data are the mean $\pm$ SD *$p < 0.05$.

radiomorphometry in the defect. The radiopacity $\pm$ SD in the untreated, ACP, O25A75, O50A50, O75A25, and OCP treated areas was $33.6 \pm 8.6\%$, $63.2 \pm 11.8\%$, $79.3 \pm 6.7\%$, $71.9 \pm 8.6\%$, $71.8 \pm 8.2\%$, and $59.2 \pm 3.5\%$, respectively. A significant difference was observed between the untreated and implanted groups. Moreover, the radiopacity of O25A75 was significantly higher than the OCP and ACP implanted groups ($p < 0.05$).

Histological and Histomorphometric Examination 8 Weeks Postimplantation. Figure 5 shows the histological section of OCP, ACP, and their mixtures at 8 weeks after implantation. New bone formation in the untreated control group was limited to the margin of the defect, and most of the defect was filled with fibrous tissue (Figure 5a). In the animals

treated with OCP, ACP, and their mixtures, newly formed bone was observed around the implanted OCP or ACP (Figure 5b–Figure 5f). This suggests that the granular radiopacity in Figure 3 corresponds to newly formed bone around the implanted granules or calcification due to the conversion from the OCP[32−34] or ACP to an apatitic phase.[22] The previous studies confirmed that OCP can be recognized as hematoxyliniphoilic substances, after the decalcification, which come from accumulated serum proteins.[1,35] It seems likely that the granule of ACP tends to remain in comparison with the granule of OCP (Figure 5).

Histomorphometric Examination 8 Weeks Postimplantation. Histomorphometric findings regarding n-Bone% are shown in Figure 6. At week 8, the n-Bone% $\pm$ SD in the untreated, ACP, O25A75, O50A50, O75A25, and OCP treated areas was $16.9 \pm 2.9\%$, $29.4 \pm 7.0\%$, $48.8 \pm 12.4\%$, $39.3 \pm 3.7\%$, $47.6 \pm 6.0\%$, and $38.2 \pm 4.3\%$, respectively. A significant difference was seen between the untreated and implanted groups without the ACP implanted group ($p < 0.05$). The n-Bone% of O25A75 was significantly higher than the ACP implanted group ($p < 0.05$).

Examination of Bone Formation for 12 Weeks. Since O25A75 enhanced the increase of the radiopacity most and the bone regeneration more than OCP and ACP alone at 8 weeks, we investigated O25A75 in comparison with OCP with prolonged implantation. Figure 7a and Figure 7b show radiographic examination of the O25A75 and OCP groups at 12 weeks postimplantation. Although greater radiopacity was observed at 12 weeks postimplantation compared to 8 weeks based on the amalgamation of isolated radiopacity in both groups, the radiopacity observed for the O25A75 group was greater than that in the OCP group. Figure 7c shows the examination of radiomorphometry in the defects of animals at 12 weeks postimplantation. The radiopacity $\pm$ SD in the O25A75 and OCP treated areas was $83.8 \pm 7.3\%$ and $63.5 \pm 8.9\%$, respectively. The radiopacity of the O25A75 group was significantly higher than the OCP implanted groups ($p < 0.05$). Figure 7d and Figure 7e show histological sections of the defects from the O25A75 and OCP animals at 12 weeks postimplantation. Newly formed bone in the defect became abundant in both groups. However, the magnified view reveals that O25A75 may induce bone regeneration more than OCP (Figure 7d and Figure 7e). Histomorphometrical findings of the n-Bone% in the defect revealed that O25A75 significantly enhanced new bone formation compared to OCP (54.0 ± 5.1 vs $42.0 \pm 3.7\%$, respectively) (Figure 7f). The results from the histomorphometric examination were consistent with those of the radiomorphometric examination as shown in Figure 7c.

Immersion in SBF Solution. The changes in surface characteristics of OCP, O25A75, and ACP after immersion in SBF for 1 and 2 weeks were examined by SEM (Figure 8). Platelike morphology of OCP was relatively remained even after immersion in SBF solution (Figure 8A and Figure 8D), which has been suggested to be a pseudomorph reflecting the original OCP underwent the hydrolysis.[6] After the immersion in SBF, the surface of ACP was covered with smaller and homogeneous spherical particles (Figure 8C and Figure 8F). The SEM micrographs of O25A75 (Figure 8B and Figure 8E) show that smaller spherical particles, as observed in ACP, deposited on the mixture of the original spherical particles (most probably ACP) and the platelike particles (most probably OCP).
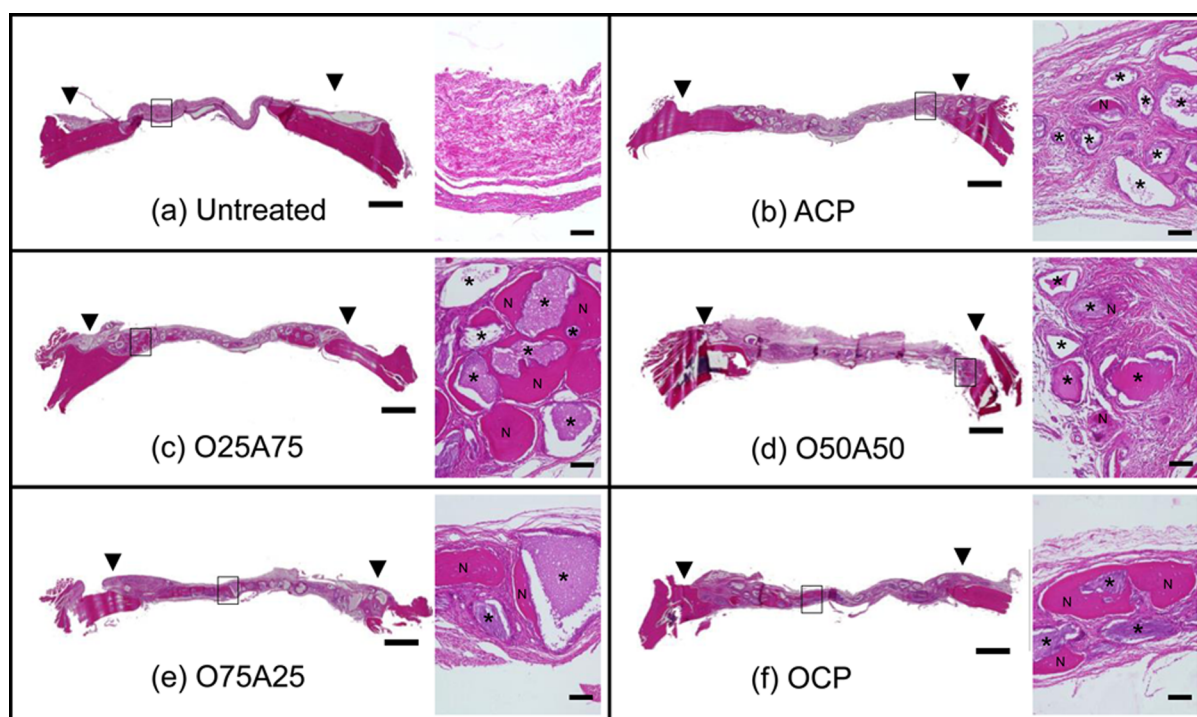
Figure 5. Overview and a magnified image of the black-lined square of the overview image of the sections stained with hematoxylin and eosin at 8 weeks postimplantation: (a) untreated control group, (b) ACP, (c) O25A75, (d) O50A50, (e) O75A25, and (f) OCP. The implantations were assessed after 8 weeks. ▼, defect margin. Bars with overview = 1 mm, and bars with magnified image = 100 μm. N, newly formed bone; *, implanted OCP or ACP.
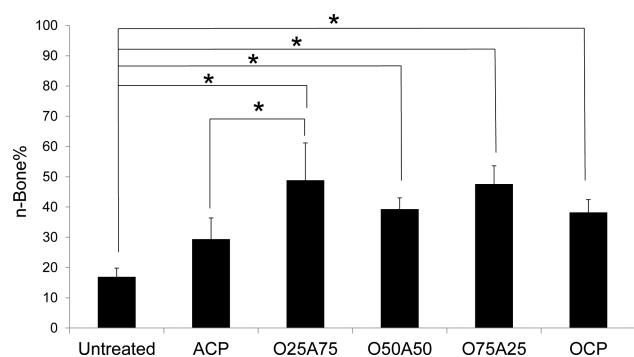

Figure 6. Quantitative analysis of the percentage of new bone in the defect (n-Bone%) at 8 weeks postimplantation of ACP, OCP/ACP mixtures, or ACP. Data are the mean ± SD *$p < 0.05$.

Figure 9 shows the XRD pattern of the OCP, O25A75, and ACP immersed in SBF for 1 and 2 weeks. The OCP structure tended to change to that of HA with a reduction in the peak intensity of the $(1\ 0\ 0)$ reflection at $2\theta = 4.9°$ over time. In the ACP and O25A75 groups, the characteristic peaks of HA were observed over time. These results suggest that OCP, ACP, and their mixture tend to be converted to an apatite structure by incubation in SBF solution.

Table 2 shows the DS of the SBF before and after the immersion of OCP, O25A75, and ACP. The results showed that the DS of all solutions examined was supersaturated with respect to HA but undersaturated with respect to DCPD. The DS of ACP decreased with respect to HA and became saturated with respect to OCP after 2 weeks. The DS of OCP decreased with respect to HA but remained slightly supersaturated with respect to OCP even after 2 weeks. The DS of O25A75 after 1 week of incubation was lower than ACP with respect to HA but

relatively comparable after 2 weeks. However, the DS of O25A75 became saturated with respect to OCP at both 1 and 2 weeks. These results indicated that O25A75 had a higher potential to convert to OCP as well as that by ACP only and tended to form OCP, while OCP remains to a condition slightly supersaturated with respect to OCP. The results indicate that ACP and O25A75 tend to saturate with respect to the OCP phase in terms of the solution composition, but the structure of both materials examined by XRD changed to that of HA. On the other hand, OCP does not attain the saturation completely with respect to the OCP phase, although the structure of this material by XRD tended to change to HA (Figure 9), indicating that the conversion from OCP to HA did not complete in terms of the solution composition. Since it has been proposed that OCP to HA conversion takes place by a hydrolytic process within the OCP structure and not only dissolution-reprecipitation process,[6,7,36−38] the present analytical results by this solution DS and the solid XRD may include such multiple conversion processes.

Figure 10 shows FTIR spectra of ACP, O25A75, and OCP before and after 2 weeks of immersion in SBF. The results indicated that OCP, ACP, and their mixture tended to convert to an apatite structure by incubation in SBF solution, which corresponded to the changes in the XRD patterns.

Figure 11 shows the curve fitting of OCP, ACP, and O25A75 before and after 1 and 2 weeks of immersion in SBF. As reported in the previous studies, apatitic and nonapatitic HPO_4^{2-} ions were detected around 550 and 530 cm^{-1}. Apatitic OH^- ions were also observed around 630 cm^{-1}. FTIR fitting analyses showed that the apatitic PO_4^{3-} ions at 575 and 600 cm^{-1} peaks increased both in ACP and O25A75 as the immersion time increased, indicating advancement of the crystallization into HA formation. However, little change was
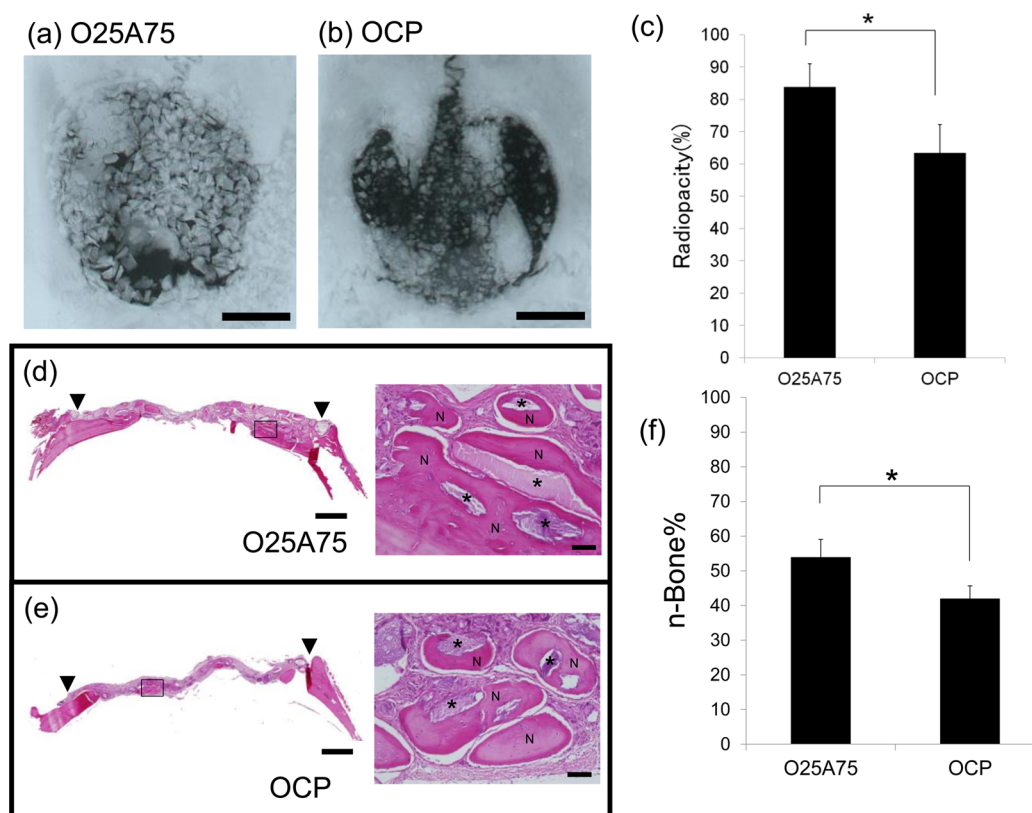
Figure 7. Radiographs of rat calvarial defects with O25A75 (a) or OCP (b) implantations after 12 weeks. Bars = 3 mm. Quantitative analysis of the percentage of radiopacity in the defect after 12 weeks (c). *$p < 0.05$. Overview and a magnified image of the black-lined square of the overview image of the sections stained with hematoxylin and eosin at 12 weeks postimplantation: (d) O25A75 or (e) OCP. ▼, defect margin. Bars with overview = 1 mm, and bars with magnified image = 100 μm. N, newly formed bone; *, implanted OCP or ACP. Quantitative analysis of the percentage of new bone in the defect (n-Bone%) at 12 weeks postimplantation (f). *$p < 0.05$.
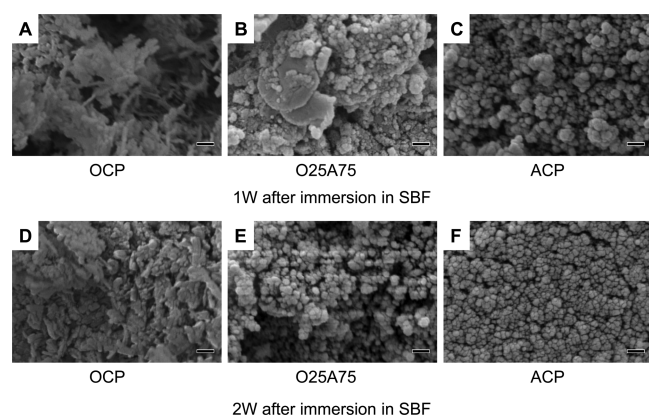

Figure 8. Scanning electron micrographs of OCP immersed in SBF for 1 week (A) or 2 weeks (D), O25A75 immersed in SBF for 1 week (B) or 2 weeks (E), and ACP immersed in SBF for 1 week (C) or 2 weeks (F). Bars = 1 μm.
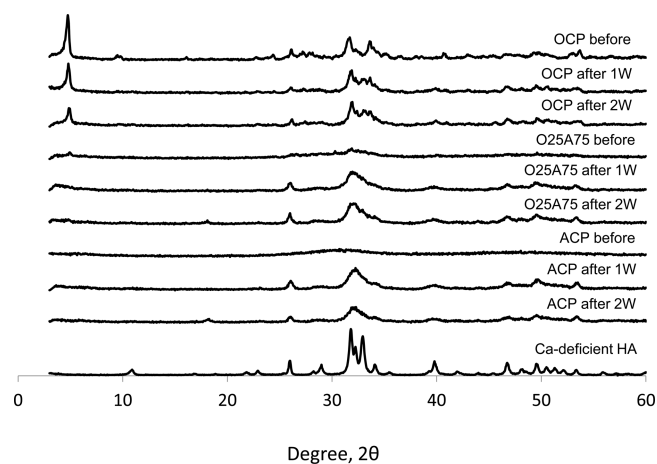

Figure 9. Changes in the XRD pattern of granules before and after immersion in SBF for 1 or 2 weeks. The XRD pattern of Ca-deficient HA was shown as a control material.

discernible for OCP, even after 2 weeks of immersion. The peak height ratios at 630 to 530 cm^{-1}, which are indicators of OH in an apatite structure, progressively increased in ACP (from 0.42 to 4.02) and O25A75 (0.51 to 4.29) but only slightly increased in OCP (from 0.71 to 1.37) before and after the immersion for 2 weeks ($n = 2$ in the same experiment; the representative tendency is described here). In contrast, the peak ratios at 530 to 550 cm^{-1}, which are indicators of nonapatitic HPO$_4^{2-}$, remained unchanged in ACP (from 0.20 to 0.32) and slightly decreased in O25A75 (from 0.59 to 0.24) but modestly

decreased in OCP (from 1.91 to 1.20) ($n = 2$ in the same experiment; the representative tendency is described here). These results indicate that the hydrolysis of OCP into HA advances very slowly, while ACP is converted to HA relatively rapidly. The hydrolysis of O25A75 could be explained by the rapid conversion of ACP and the enhancement of the modest decrease of HPO$_4$, which may be controlled by the hydrolysis reaction of ACP occurring in the vicinity around OCP.

Table 2. Solution Composition and Degree of Supersaturation (DS) of Simulated Body Fluid (SBF) before and after the Immersion of OCP, ACP, and the Mixture (O25A75)

		concentration[a] (mM)		DS at pH 7.40 and 37 °C		
		calcium	phosphate	HA	OCP	DCPD
SBF original		2.41 ± 0.01	1.01 ± 0.01	9.46×10^{11}	2.30×10^{3}	6.46×10^{-1}
ACP	1W	3.02 ± 0.044	0.29 ± 0.0051	7.13×10^{10}	1.36×10^{2}	2.32×10^{-1}
	2W	1.29 ± 0.010	0.18 ± 0.036	2.95×10^{8}	1.30×10^{0}	6.53×10^{-2}
O25A75	1w	0.84 ± 0.083	0.33 ± 0.012	2.19×10^{8}	1.49×10^{0}	7.88×10^{-2}
	2w	1.20 ± 0.023	0.32 ± 0.058	1.14×10^{9}	5.46×10^{0}	1.08×10^{-1}
OCP	1W	1.60 ± 0.010	0.59 ± 0.010	2.79×10^{10}	1.01×10^{2}	2.60×10^{-1}
	2W	1.25 ± 0.024	0.50 ± 0.041	5.19×10^{9}	2.39×10^{1}	1.75×10^{-1}

[a]The calcium and phosphate concentrations in "SBF original" are averages from three independent analyses from one SBF solution. Those in the experimental solutions are the average from three independent immersions of the calcium phosphate.
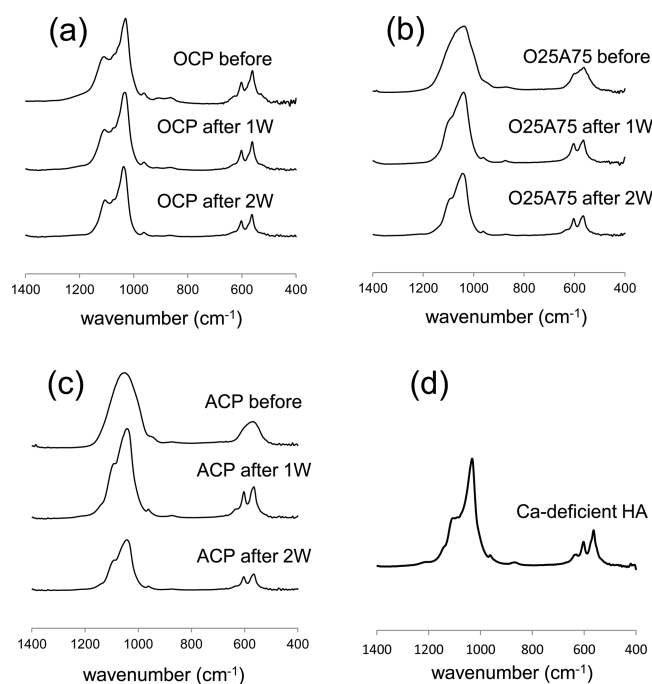

Figure 10. Changes in the FTIR spectra of granules before and after immersion in SBF for 1 or 2 weeks. (a) OCP, (b) O25A75, (c) ACP, or Ca-deficient HA (d).

■ DISCUSSION

It has been reported that OCP and ACP exhibits osteoconductivity, respectively, if implanted in the subperiosteal region of mouse calvaria, but new bone forms on OCP more quickly than on ACP.[22] The present study found that the osteoconductivities of OCP and ACP respectively can be augmented if OCP was mixed with ACP in the range from 25 wt % OCP to 75 wt % OCP with ACP and when they are coimplanted in critical-sized rat calvaria defects. The copresence of ACP with OCP affected the conversion process of OCP into HA as clearly shown by the DS estimation from the SBF immersion experiment. The surface of the O25A75 after the SBF immersion changed to the surface different than both the respective original surfaces of OCP and ACP after the SBF immersion. These results indicate that the extent of conversion of OCP into HA in vivo is controlled by the presence of ACP and suggests that the apatitic materials formed from the conversion contributes to increase the extent of osteoconductivity of OCP.

The osteoconductivity of O25A75 was higher than ACP and OCP by the radiographically and higher than ACP histomorphometrically at 8 weeks significantly. However, the effect was not clear between the mixing ratios from 25 wt % OCP to 75 wt % of OCP with ACP. It is still unclear why the mixing of ACP into OCP enhances the osteoconductivity compared to the single phase of these materials. We investigated the possible mechanism underlying the intrinsic metastable properties of OCP and ACP under physiological conditions. The XRD analysis of the implanted and then retrieved OCP, ACP, and their mixtures at 2 weeks post-implantation confirmed that they corresponded to the low crystalline HA phase. The rate of conversion from high to low was ACP, OCP/ACP, and OCP, respectively. ACP was not dissolved completely by its implantation in rat critical-sized calvaria defects, as shown in the histological findings, which was consistent with previous work of subperiosteal implantation of ACP onto mouse calvaria.[22] This could be due to the use of relatively large ACP granules in the present study. The results by the histological examination (Figure 7d and Figure 7e) suggested that bone formation was enhanced by the advancement of the biodegradation of OCP coupled with new bone deposition, which is a property of OCP as previously reported.[39,40] On the other hand, ACP may have a role to provide the osteoconductive surface for the new bone formation.

It is known that ACP exhibits a variety of Ca/P molar ratios that range from 1.15[41] to 1.5.[13] The physicochemical and the bioactive properties of ACPs have been well described in relation to the structure.[13] ACP has been recently recognized as an active material that shows osteoinduction by increasing local calcium concentration through the involvement of connexin 43-gap junction in a three-dimensional dental pulp cell construct.[23] Our previous study found that ACP is an osteoconductive material when placed onto mouse calvaria and can directly bind new bone tissue; however, the appearance of new bone occurs more quickly on OCP than ACP, despite the crystal phase of both materials being converted to HA.[22] A chemical study revealed that ACP transformed to HA via an OCP-like phase.[5] Although the OCP-like phase is a transitory phase that rapidly transforms to HA,[5] the characteristics of the OCP-like phase are different from the well-crystallized OCP used in the present study.[1,7] The chemical relationship between ACP and OCP has been previously reported based on a mechanistic model of HA formation from supersaturated solution using a cluster theory of nano-ACP particles.[18,19] The present study did not analyze how the presence of ACP affects the structural relationship between ACP and OCP. However, it is likely that the control of
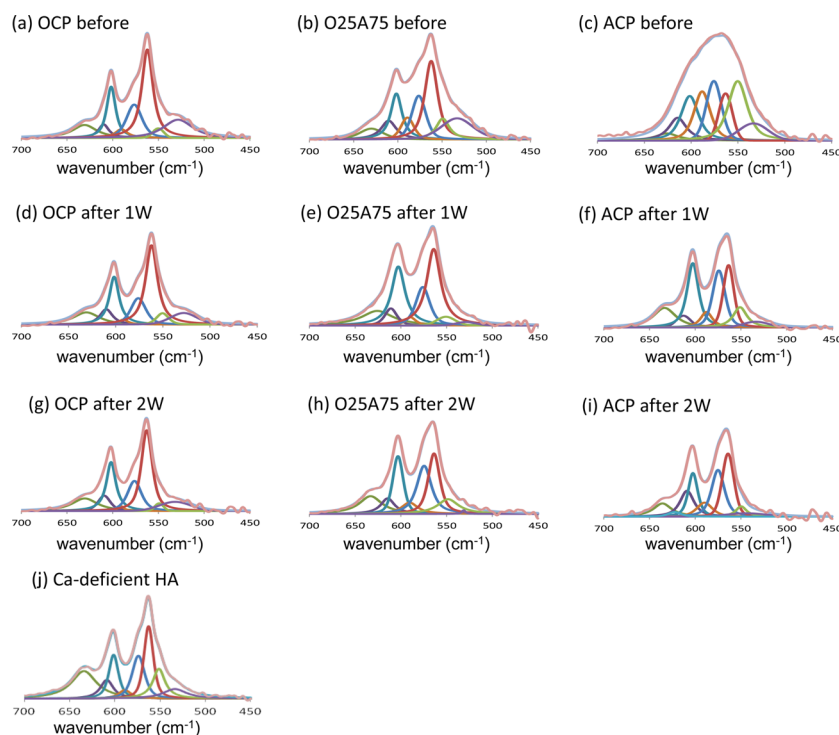
Figure 11. FTIR spectral curve fitting of OCP (a, d, g), O25A75 (b, e, h), or ACP (c, f, i) before and after immersion into SBF for 2 weeks. A spectrum of Ca-deficient HA was shown as a control material (j).

the conversion is associated with the osteoconduction of OCP: the osteoconductive property of OCP is in fact augmented together with the enhancement of conversion of OCP to HA. Our recent study confirmed that the reduction of calcium concentration around OCP crystals increased phosphorylation of p38 in osteoblastic signaling, which is a possible mechanism of OCP to enhance osteoblast activation[42] and could be related in the present stimulatory capacity of OCP with ACP.

It is interesting to further understand not only the structural relationship but also the surface structural changes of OCP that could directly affect the tissue response. SEM observation found that the surface morphology of O25A75 differs from the respective original surface of OCP and ACP. FTIR curve fitting analysis showed that the conversions of OCP and the mixture of OCP and ACP (O25A75) had similar surface characteristics that increased the surface apatitic hydroxide and decreased the acid phosphate species. The latter change corresponded to the hydrolysis of OCP into HA as determined by chemical analyses[7,10] or FTIR spectroscopic analysis.[26] These surface structural changes and motifs induce a distinct adsorption affinity of serum proteins onto OCP[7,9,43] and specific interactions of small molecules with HA.[44] Thus, they may lead to the distinct osteoconductive properties observed between OCP and HA,[1,45] which could explain in part the increase in osteoconductivity of OCP enhanced by the introduction of ACP.

The in vitro immersion study of OCP, ACP, and the mixture (O25A75) in SBF indicated that the conversion advancement was similar under in vitro and in vivo conditions. The calculation of solution saturation (DS) after the immersions reflects the rate of the HA formation. The DS decreased the most so as to become saturated with respect to HA in the introduction of ACP alone. DS remained relatively constant after OCP was introduced, indicating that SBF does not accelerate the conversion of OCP. This finding is in agreement with previous works showing that SBF becomes saturated with OCP quickly before hydrolysis begins.[46−48] In contrast, the copresence of ACP with OCP reduced the DS with respect to HA and OCP after 1 week of incubation and became similar to that of ACP after 2 weeks of incubation, indicating that the OCP conversion in the mixture is accelerated earlier than that by OCP alone. These results suggest that ACP contributes to enhance the OCP conversion by providing calcium and phosphate ions to OCP in SBF. It is also probable that ACP may contribute to the conversion of OCP by changing pH locally: the local increase of pH through the dissolution of ACP catalyzes transformation of OCP to HA-catalytic hydrolysis.[5,6,14,16] Taken together, it is reasonable to postulate that the observed increase in bone regeneration of rat critical-sized calvaria defects by mixing ACP with OCP is associated with the newly deposited crystals on the surface of OCP and ACP as a result of the conversion of these materials and possibly soluble ions from the loaded ACP for OCP.

■ CONCLUSIONS

In conclusion, the present study provided a mechanism for the improvement of the osteoconduction of calcium phosphate materials and in particular the osteoconductive properties of OCP bone substitute material. The rate of conversion from OCP into HA can be accelerated in the presence of ACP as a secondary phase and is likely to be the cause of the osteoconduction of OCP. The present study may also provide a clue to develop further highly osteoconductive calcium phosphate ceramics as bone substitute materials.

■ AUTHOR INFORMATION

Corresponding Author

*Phone:+81-22-717-7635. Fax: +81-22-717-7637. E-mail: suzuki-o@m.tohoku.ac.jp.

Notes

The authors declare no competing financial interest.

■ REFERENCES

(1) Suzuki, O.; Kamakura, S.; Katagiri, T.; Nakamura, M.; Zhao, B.; Honda, Y.; Kamijo, R. Bone Formation Enhanced by Implanted Octacalcium Phosphate Involving Conversion into Ca-Deficient Hydroxyapatite. *Biomaterials* **2006**, *27*, 2671−2681.

(2) Anada, T.; Kumagai, T.; Honda, Y.; Masuda, T.; Kamijo, R.; Kamakura, S.; Yoshihara, N.; Kuriyagawa, T.; Shimauchi, H.; Suzuki, O. Dose-Dependent Osteogenic Effect of Octacalcium Phosphate on Mouse Bone Marrow Stromal Cells. *Tissue Eng., Part A* **2008**, *14*, 965−78.

(3) Brown, W. E. Crystal Growth of Bone Mineral. *Clin. Orthop. Relat. Res.* **1966**, *44*, 205−220.

(4) Brown, W. E.; Smith, J. P.; Lehr, J. R.; Frazier, A. W. Crystallographic and Chemical Relations between Octacalcium Phosphate and Hydroxyapatite. *Nature* **1962**, *196*, 1050−1055.

(5) Meyer, J. L.; Eanes, E. D. A Thermodynamic Analysis of the Amorphous to Crystalline Calcium Phosphate Transformation. *Calcif. Tissue Res.* **1978**, *25*, 59−68.

(6) Brown, W. E.; Mathew, M.; Tung, M. S. Crystal Chemistry of Octacalcium Phosphate. *Prog. Cryst. Growth Charact.* **1981**, *4*, 59−87.

(7) Suzuki, O.; Yagishita, H.; Yamazaki, M.; Aoba, T. Adsorption of Bovine Serum Albumin onto Octacalcium Phosphate and Its Hydrolyzates. *Cells Mater.* **1995**, *5*, 45−54.

(8) Suzuki, O.; Kamakura, S.; Katagiri, T. Surface Chemistry and Biological Responses to Synthetic Octacalcium Phosphate. *J. Biomed. Mater. Res., Part B* **2006**, *77*, 201−12.

(9) Shiwaku, Y.; Anada, T.; Yamazaki, H.; Honda, Y.; Morimoto, S.; Sasaki, K.; Suzuki, O. Structural, Morphological and Surface Characteristics of Two Types of Octacalcium Phosphate-Derived Fluoride-Containing Apatitic Calcium Phosphates. *Acta Biomater.* **2012**, *8*, 4417−4425.

(10) Suzuki, O.; Yagishita, H.; Amano, T.; Aoba, T. Reversible Structural Changes of Octacalcium Phosphate and Labile Acid Phosphate. *J. Dent. Res.* **1995**, *74*, 1764−1769.

(11) Moreno, E. C.; Aoba, T. Comparative Solubility Study of Human Dental Enamel, Dentin, and Hydroxyapatite. *Calcif. Tissue Int.* **1991**, *49*, 6−13.

(12) Moreno, E. C.; Kresak, M.; Zahradnik, R. T. Fluoridated Hydroxyapatite Solubility and Caries Formation. *Nature* **1974**, *247*, 64−5.

(13) Combes, C.; Rey, C. Amorphous Calcium Phosphates: Synthesis, Properties and Uses in Biomaterials. *Acta Biomater.* **2010**, *6*, 3362−78.

(14) Eanes, E. D.; Gillessen, I. H.; Posner, A. S. Intermediate States in the Precipitation of Hydroxyapatite. *Nature* **1965**, *208*, 365−7.

(15) Mahamid, J.; Aichmayer, B.; Shimoni, E.; Ziblat, R.; Li, C.; Siegel, S.; Paris, O.; Fratzl, P.; Weiner, S.; Addadi, L. Mapping Amorphous Calcium Phosphate Transformation into Crystalline Mineral from the Cell to the Bone in Zebrafish Fin Rays. *Proc. Natl. Acad. Sci. U. S. A.* **2010**, *107*, 6316−6321.

(16) Termine, J. D.; Eanes, E. D. Comparative Chemistry of Amorphous and Apatitic Calcium Phosphate Preparations. *Calcif. Tissue Res.* **1972**, *10*, 171−97.

(17) Dey, A.; Bomans, P. H. H.; Muller, F. A.; Will, J.; Frederik, P. M.; de With, G.; Sommerdijk, N. A. J. M. The Role of Prenucleation Clusters in Surface-Induced Calcium Phosphate Crystallization. *Nat. Mater.* **2010**, *9*, 1010−1014.

(18) Habraken, W. J.; Tao, J.; Brylka, L. J.; Friedrich, H.; Bertinetti, L.; Schenk, A. S.; Verch, A.; Dmitrovic, V.; Bomans, P. H.; Frederik, P. M.; Laven, J.; van der Schoot, P.; Aichmayer, B.; de With, G.; DeYoreo, J. J.; Sommerdijk, N. A. Ion-Association Complexes Unite Classical and Non-Classical Theories for the Biomimetic Nucleation of Calcium Phosphate. *Nat. Commun.* **2013**, *4*, 1507.

(19) Onuma, K.; Ito, A. Cluster Growth Model for Hydroxyapatite. *Chem. Mater.* **1998**, *10*, 3346−3351.

(20) He, W.; Andersson, M.; de Souza, P. P.; de Souza Costa, C. A.; Munoz, E. M.; Schwartz-Filho, H. O.; Hayashi, M.; Hemdal, A.; Fredel, A.; Wennerberg, A.; Jimbo, R. Osteogenesis-Inducing Calcium Phosphate Nanoparticle Precursors Applied to Titanium Surfaces. *Biomed. Mater.* **2013**, *8*, 035007.

(21) Rey, C.; Hina, A.; Somrani, S.; Jemal, M.; Glimcher, M. J. Chemical Properties of Poorly Crystalline Apatites. *Phosphorus Res. Bull.* **1996**, *6*, 67−70.

(22) Suzuki, O.; Nakamura, M.; Miyasaka, Y.; Kagayama, M.; Sakurai, M. Bone Formation on Synthetic Precursors of Hydroxyapatite. *Tohoku J. Exp. Med.* **1991**, *164*, 37−50.

(23) Syed-Picard, F. N.; Jayaraman, T.; Lam, R. S.; Beniash, E.; Sfeir, C. Osteoinductivity of Calcium Phosphate Mediated by Connexin 43. *Biomaterials* **2013**, *34*, 3763−74.

(24) Tao, J.; Pan, H.; Zeng, Y.; Xu, X.; Tang, R. Roles of Amorphous Calcium Phosphate and Biological Additives in the Assembly of Hydroxyapatite Nanoparticles. *J. Phys. Chem. B* **2007**, *111*, 13410−8.

(25) Kokubo, T.; Kushitani, H.; Sakka, S.; Kitsugi, T.; Yamamuro, T. Solutions Able to Reproduce in Vivo Surface-Structure Changes in Bioactive Glass-Ceramic a-W. *J. Biomed. Mater. Res.* **1990**, *24*, 721−34.

(26) Vandecandelaere, N.; Rey, C.; Drouet, C. Biomimetic Apatite-Based Biomaterials: On the Critical Impact of Synthesis and Post-Synthesis Parameters. *J. Mater. Sci.: Mater. Med.* **2012**, *23*, 2593−606.

(27) Moreno, E. C.; Margolis, H. C. Composition of Human Plaque Fluid. *J. Dent. Res.* **1988**, *67*, 1181−9.

(28) Aoba, T.; Moreno, E. C. The Enamel Fluid in the Early Secretory Stage of Porcine Amelogenesis: Chemical Composition and Saturation with Respect to Enamel Mineral. *Calcif. Tissue Int.* **1987**, *41*, 86−94.

(29) Moreno, E. C.; Aoba, T. Calcium Bonding in Enamel Fluid and Driving Force for Enamel Mineralization in the Secretory Stage of Amelogenesis. *Adv. Dent. Res.* **1987**, *1*, 245−51.

(30) Tung, M. S.; Eidelman, N.; Sieck, B.; Brown, W. E. Octacalcium Phosphate Solubility Product from 4 to 37 °C. *J. Res. Natl. Bur. Stand.* **1988**, *93*, 613−624.

(31) Mathew, M.; Brown, W.; Schroeder, L.; Dickens, B. Crystal Structure of Octacalcium Bis(Hydrogenphosphate) Tetrakis-(Phosphate)Pentahydrate, $Ca_8(HPO_4)_2(PO_4)_4 \cdot 5H_2O$. *J. Crystallogr. Spectrosc. Res.* **1988**, *18*, 235−250.

(32) Kamakura, S.; Sasaki, K.; Honda, Y.; Anada, T.; Matsui, K.; Echigo, S.; Suzuki, O. Dehydrothermal Treatment of Collagen Influences on Bone Regeneration by Octacalcium Phosphate (Ocp) Collagen Composites. *J. Tissue Eng. Regener. Med.* **2007**, *1*, 450−6.

(33) Suzuki, Y.; Kamakura, S.; Honda, Y.; Anada, T.; Hatori, K.; Sasaki, K.; Suzuki, O. Appositional Bone Formation by OCP-Collagen Composite. *J. Dent. Res.* **2009**, *88*, 1107−1112.

(34) Tanuma, Y.; Anada, T.; Honda, Y.; Kawai, T.; Kamakura, S.; Echigo, S.; Suzuki, O. Granule Size-Dependent Bone Regenerative Capacity of Octacalcium Phosphate in Collagen Matrix. *Tissue Eng., Part A* **2012**, *18*, 546−57.

(35) Suzuki, O.; Nakamura, M.; Miyasaka, Y.; Kagayama, M.; Sakurai, M. Maclura Pomifera Agglutinin-Binding Glycoconjugates on Converted Apatite from Synthetic Octacalcium Phosphate Implanted

into Subperiosteal Region of Mouse Calvaria. *Bone Miner.* **1993**, *20*, 151−66.

(36) LeGeros, R. Z.; Daculsi, G.; Orly, I.; Abergas, T.; Torres, W. Solution-Mediated Transformation of Octacalcium Phosphate (Ocp) to Apatite. *Scanning Electron Microsc.* **1989**, *3*, 129−138.

(37) Suzuki, O.; Imaizumi, H.; Kamakura, S.; Katagiri, T. Bone Regeneration by Synthetic Octacalcium Phosphate and Its Role in Biological Mineralization. *Curr. Med. Chem.* **2008**, *15*, 305−313.

(38) Tomazic, B. B.; Tung, M. S.; Gregory, T. M.; Brown, W. E. Mechanism of Hydrolysis of Octacalcium Phosphate. *Scanning Microsc.* **1989**, *3*, 119−127.

(39) Imaizumi, H.; Sakurai, M.; Kashimoto, O.; Kikawa, T.; Suzuki, O. Comparative Study on Osteoconductivity by Synthetic Octacalcium Phosphate and Sintered Hydroxyapatite in Rabbit Bone Marrow. *Calcif. Tissue Int.* **2006**, *78*, 45−54.

(40) Takami, M.; Mochizuki, A.; Yamada, A.; Tachi, K.; Zhao, B.; Miyamoto, Y.; Anada, T.; Honda, Y.; Inoue, T.; Nakamura, M.; Suzuki, O.; Kamijo, R. Osteoclast Differentiation Induced by Synthetic Octacalcium Phosphate through Rankl Expression in Osteoblasts. *Tissue Eng., Part A* **2009**, *15*, 3991−4000.

(41) Wuthier, R. E.; Rice, G. S.; Wallace, J. E., Jr; Weaver, R. L.; LeGeros, R. Z.; Eanes, E. D. In Vitro Precipitation of Calcium Phosphate under Intracellular Conditions: Formation of Brushite from an Amorphous Precursor in the Absence of Atp. *Calcif. Tissue Int.* **1985**, *37*, 401−10.

(42) Nishikawa, R.; Anada, T.; Ishiko-Uzuka, R.; Suzuki, O. Osteoblastic Differentiation of Stromal ST-2 Cells from Octacalcium Phosphate Exposure via p38 Signaling Pathway. *Dent. Mater. J.* **2014**, *33*, 242−51.

(43) Kaneko, H.; Kamiie, J.; Kawakami, H.; Anada, T.; Honda, Y.; Shiraishi, N.; Kamakura, S.; Terasaki, T.; Shimauchi, H.; Suzuki, O. Proteome Analysis of Rat Serum Proteins Adsorbed onto Synthetic Octacalcium Phosphate Crystals. *Anal. Biochem.* **2011**, *418*, 276−85.

(44) Errassifi, F.; Sarda, S.; Barroug, A.; Legrouri, A.; Sfihi, H.; Rey, C. Infrared, Raman and NMR Investigations of Risedronate Adsorption on Nanocrystalline Apatites. *J. Colloid Interface Sci.* **2014**, *420*, 101−11.

(45) Miyatake, N.; Kishimoto, K. N.; Anada, T.; Imaizumi, H.; Itoi, E.; Suzuki, O. Effect of Partial Hydrolysis of Octacalcium Phosphate on Its Osteoconductive Characteristics. *Biomaterials* **2009**, *30*, 1005−14.

(46) Ito, N.; Kamitakahara, M.; Yoshimura, M.; Ioku, K. Importance of Nucleation in Transformation of Octacalcium Phosphate to Hydroxyapatite. *Mater. Sci. Eng., C* **2014**, *40*, 121−6.

(47) Lu, X.; Leng, Y. Theoretical Analysis of Calcium Phosphate Precipitation in Simulated Body Fluid. *Biomaterials* **2005**, *26*, 1097−108.

(48) Yokoi, T.; Kim, I. Y.; Ohtsuki, C. Mineralization of Calcium Phosphate on Octacalcium Phosphate in a Solut Mineralization of Calcium Phosphate on Octacalcium Phosphate in a Solution Mimicking in vivo Conditions. *Phosphorus Res. Bull.* **2012**, *26*, 71−6.

22611

dx.doi.org/10.1021/am5067139 | *ACS Appl. Mater. Interfaces* 2014, 6, 22602−22611